Ferroptosis as a target for protection against cardiomyopathy

Xuexian Fang[a], Hao Wang[a,b], Dan Han[a], Enjun Xie[a], Xiang Yang[a], Jiayu Wei[a], Shanshan Gu[c,d], Feng Gao[e], Nali Zhu[f,g], Xiangju Yin[a], Qi Cheng[a], Pan Zhang[a], Wei Dai[a], Jinghai Chen[e], Fuquan Yang[f,g], Huang-Tian Yang[c,d], Andreas Linkermann[h,1], Wei Gu[i,j,1], Junxia Min[a,1], and Fudi Wang[a,b,1]

[a]The First Affiliated Hospital, School of Public Health, Institute of Translational Medicine, Zhejiang University School of Medicine, 310058 Hangzhou, China; [b]Department of Nutrition, Precision Nutrition Innovation Center, School of Public Health, Zhengzhou University, 450001 Zhengzhou, China; [c]Key Laboratory of Stem Cell Biology, Institute of Health Sciences, Shanghai Jiao Tong University School of Medicine and Shanghai Institutes for Biological Sciences, Chinese Academy of Sciences, 200031 Shanghai, China; [d]Laboratory of Molecular Cardiology, Institute of Health Sciences, Shanghai Jiao Tong University School of Medicine and Shanghai Institutes for Biological Sciences, Chinese Academy of Sciences, 200031 Shanghai, China; [e]The Second Affiliated Hospital, Institute of Translational Medicine, Zhejiang University School of Medicine, 310020 Hangzhou, China; [f]Laboratory of Protein and Peptide Pharmaceuticals, Institute of Biophysics, Chinese Academy of Sciences and University of Chinese Academy of Sciences, 100101 Beijing, China; [g]Laboratory of Proteomics, Institute of Biophysics, Chinese Academy of Sciences and University of Chinese Academy of Sciences, 100101 Beijing, China; [h]Department of Nephrology, Medical Clinic 3, University Hospital Carl Gustav Carus at the Technische Universität Dresden, 01307 Dresden, Germany; [i]Institute for Cancer Genetics, Herbert Irving Comprehensive Cancer Center, College of Physicians and Surgeons, Columbia University, New York, NY 10032; and [j]Department of Pathology and Cell Biology, Herbert Irving Comprehensive Cancer Center, College of Physicians and Surgeons, Columbia University, New York, NY 10032

Edited by Tak W. Mak, The Campbell Family Institute for Breast Cancer Research at Princess Margaret Cancer Centre, University Health Network, Toronto, Ontario, Canada, and approved January 4, 2019 (received for review December 12, 2018)

Heart disease is the leading cause of death worldwide. A key pathogenic factor in the development of lethal heart failure is loss of terminally differentiated cardiomyocytes. However, mechanisms of cardiomyocyte death remain unclear. Here, we discovered and demonstrated that ferroptosis, a programmed iron-dependent cell death, as a mechanism in murine models of doxorubicin (DOX)- and ischemia/reperfusion (I/R)-induced cardiomyopathy. In canonical apoptosis and/or necroptosis-defective *Ripk3*$^{-/-}$, *Mlkl*$^{-/-}$, or *Fadd*$^{-/-}$*Mlkl*$^{-/-}$ mice, DOX-treated cardiomyocytes showed features of typical ferroptotic cell death. Consistently, compared with dexrazoxane, the only FDA-approved drug for treating DOX-induced cardiotoxicity, inhibition of ferroptosis by ferrostatin-1 significantly reduced DOX cardiomyopathy. RNA-sequencing results revealed that heme oxygenase-1 (*Hmox1*) was significantly up-regulated in DOX-treated murine hearts. Administering DOX to mice induced cardiomyopathy with a rapid, systemic accumulation of nonheme iron via heme degradation by Nrf2-mediated up-regulation of Hmox1, which effect was abolished in *Nrf2*-deficent mice. Conversely, zinc protoporphyrin IX, an Hmox1 antagonist, protected the DOX-treated mice, suggesting free iron released on heme degradation is necessary and sufficient to induce cardiac injury. Given that ferroptosis is driven by damage to lipid membranes, we further investigated and found that excess free iron accumulated in mitochondria and caused lipid peroxidation on its membrane. Mitochondria-targeted antioxidant MitoTEMPO significantly rescued DOX cardiomyopathy, supporting oxidative damage of mitochondria as a major mechanism in ferroptosis-induced heart damage. Importantly, ferrostatin-1 and iron chelation also ameliorated heart failure induced by both acute and chronic I/R in mice. These findings highlight that targeting ferroptosis serves as a cardioprotective strategy for cardiomyopathy prevention.

ferroptosis | iron | heart injury | cell death | mitochondria

Cell death is a fundamental physiological process involved in development, aging, and tissue homeostasis, and often dysregulated in various pathological conditions (1). As the first-discovered form of regulated cell death, caspase-dependent apoptosis has been the focus of mechanism research and drug target for decades; however, recent studies have discovered regulatory mechanisms and signaling pathways for previously unrecognized forms of regulated cell death (2). Ferroptosis is a novel form of regulated cell death characterized by the iron-dependent accumulation of lipid peroxides to lethal levels, which is morphologically, biochemically, and genetically distinct from apoptosis, necroptosis, and autophagy (3, 4). Ferroptosis has been implicated in the pathological process associated with carcinogenesis, degenerative diseases, stroke, and kidney ischemia/reperfusion (I/R) injury (5, 6).

Anthracyclines, which comprise a class of drugs that includes doxorubicin (DOX), daunorubicin, epirubicin, and idarubicin, are commonly used to treat breast cancer, leukemia, and many other types of malignancies (7). However, the clinical use of anthracyclines is limited by its cardiotoxic effects, which can include irreversible degenerative cardiomyopathy and congestive heart failure (8). Based on an analysis of three separate phase III clinical trials, an estimated 26% of cancer patients develop DOX-related congestive heart failure following a cumulative dose of 550 mg/m^2 (9); moreover, more than half of all elderly patients with lymphoma and survivors of childhood cancer who were treated with DOX have a high risk of developing cardiotoxicity (10).

Significance

Nonapoptotic cell death-induced tissue damage has been implicated in a variety of diseases, including neurodegenerative disorder, inflammation, and stroke. In this study, we demonstrate that ferroptosis, a newly defined iron-dependent cell death, mediates both chemotherapy- and ischemia/reperfusion-induced cardiomyopathy. RNA-sequencing analysis revealed up-regulation of heme oxygenase 1 by doxorubicin as a major mechanism of ferroptotic cardiomyopathy. As a result, heme oxygenase 1 degrades heme and releases free iron in cardiomyocytes, which in turn leads to generation of oxidized lipids in the mitochondria membrane. Most importantly, both iron chelation therapy and pharmacologically blocking ferroptosis could significantly alleviate cardiomyopathy in mice. These findings suggest targeting ferroptosis as a strategy for treating deadly heart disease.

Author contributions: X.F. and F.W. designed research; X.F., H.W., D.H., E.X., X. Yang, J.W., S.G., F.G., N.Z., X. Yin, Q.C., P.Z., and W.D. performed research; J.C., F.Y., and H.-T.Y. contributed new reagents/analytic tools; X.F. and H.W. analyzed data; and X.F., A.L., W.G., J.M., and F.W. wrote the paper.

The authors declare no conflict of interest.

This article is a PNAS Direct Submission.

[1]To whom correspondence may be addressed. Email: Andreas.Linkermann@uniklinikum-dresden.de, wg8@cumc.columbia.edu, junxiamin@zju.edu.cn, or fwang@zju.edu.cn.

This article contains supporting information online at www.pnas.org/lookup/suppl/doi:10.1073/pnas.1821022116/-/DCSupplemental.

Published online January 28, 2019.

Death of terminally differentiated cardiomyocytes is a crucial pathogenic factor in the development of heart injury. DOX has also been reported to induce various forms of cell death, including apoptosis, autophagy, necroptosis, and pyroptosis (11–14). However, inhibiting either apoptosis or necroptosis only partially improved the survival of DOX-treated cardiac cells (13), suggesting that another form of cell death likely contributes to DOX-induced cardiotoxicity. On the other hand, a growing body of evidence indicates that increased iron may play a key role in this condition (15), but the fundamental mechanisms of iron accumulation and its toxicity are poorly understood.

In the current study, we performed in vivo drug screening and demonstrated that iron-dependent ferroptosis, rather than other known forms of regulated cell death, has a crucial role in DOX-induced cardiomyopathy. Mechanistically, up-regulation of *Hmox1* via *Nrf2* activation causes heme degradation in heart and leads to release of free iron, which accumulates in mitochondria and triggers lipid peroxidation. Moreover, targeting ferroptosis also protects the heart from I/R-induced myocardial remodeling and heart failure. Our results provide insight into the pathogenic mechanisms that underlie iron overload-induced cardiomyopathy and may provide therapeutic targets for the development of improved treatment strategies.

Results

Ferroptosis Drives DOX-Induced Cardiomyopathy and Mortality in Mice. First, to investigate the relative contributions of various forms of cell death in DOX-induced cardiotoxicity, we measured survival following a single dose of DOX in mice in the absence or presence of various inhibitors of cell death (Fig. 1*A*). Our analysis revealed that the ferroptosis inhibitor Fer-1 significantly reduced DOX-induced mortality; in contrast, survival was not significantly improved in mice that received emricasan (an inhibitor of apoptosis), necrostatin-1 (Nec-1, a specific inhibitor of receptor interacting protein kinase 1-mediated necroptosis), or 3-methyladenine (3-MA, an inhibitor of autophagy).

DOX causes receptor interacting protein kinase 3 (Ripk3)-induced myocardial necroptosis independent of Ripk1 and mixed lineage kinase domain-like protein (Mlkl) has been recently reported (13). We found that DOX-induced mortality was reduced in *Ripk3*$^{-/-}$ mice compared with wild-type (WT) littermates, and treating mice with Fer-1 to block ferroptosis reduced DOX-induced mortality in *Ripk3*$^{-/-}$ mice even further, suggesting that both ferroptosis and Ripk3-mediated necroptosis play an independent role in DOX-induced cardiotoxicity (Fig. 1*B*). However, unlike the previous finding (13), we observed that Ca^{2+} calmodulin-dependent protein kinase (CaMKII) inhibition using KN-93 showed little effect on DOX-induced mortality either by single KN-93 treatment or cotreatment with Fer-1 (Fig. 1*C*). As shown in Fig. 1*D*, DOX treatment induced a robust increase in cardiac, hepatic, and renal *Ptgs2* mRNA, a putative molecular marker of ferroptosis (16), with the strongest increase (approximately threefold compared with control-treated mice) in the heart and liver.

A powerful approach to definitively study the involvement of various forms of cell death is to remove key components in specific cell death pathways. Therefore, we further generated apoptosis- and necroptosis-defective (*Mlkl*$^{-/-}$ and *Fadd*$^{-/-}$*Mlkl*$^{-/-}$) mice (17). Consistently, eliminating either Fadd-dependent apoptosis or Mlkl-dependent necroptosis had no effect on DOX-induced cardiomyopathy, as assessed by histology and by measuring serum LDH (Fig. 1 *E* and *F*).

Inhibition of Ferroptosis Prevents Against DOX-Induced Cardiac Injury. Dexrazoxane (DXZ), an iron chelator, is currently the only drug approved by the FDA for preventing DOX-induced cardiotoxicity in cancer patients. Based on the levels of cardiac *Ptgs2* mRNA (*SI Appendix*, Fig. S1*A*), serum and cardiac lipid peroxidation (*SI Appendix*, Fig. S1 *B* and *C*), it seems plausible

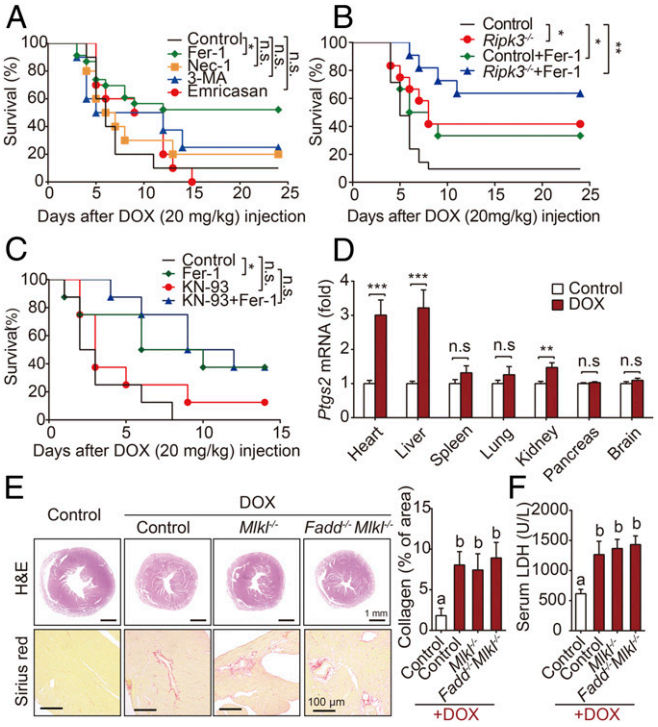

Fig. 1. Myocardial ferroptosis dominates DOX-induced mortality. (*A*) Kaplan–Meier survival curves of mice pretreated with saline (control), Fer-1 (a ferroptosis inhibitor), 3-MA (an autophagy inhibitor), emricasan (a pan-caspase inhibitor), or Nec-1 (a necroptosis inhibitor), followed by DOX (20 mg/kg, i.p.) on day 0 (n = 10–15 mice per group). (*B*) Kaplan–Meier survival curves of the indicated mice (control and *Ripk3*$^{-/-}$) treated with or without Fer-1 followed by DOX (20 mg/kg, i.p.) (n = 10–12 mice per group). (*C*) Kaplan–Meier survival curves of the indicated mice treated with KN-93 and/or Fer-1 followed by DOX (20 mg/kg, i.p.) (n = 10–12 mice per group). (*D*) Relative levels of *Ptgs2* mRNA were measured in the indicated organs injected with DOX (10 mg/kg, i.p.) or saline (control) for 4 d. (n = 8 mice per group). (*E*) Representative images and quantitative analyses of H&E and Sirius red staining of heart sections in control, *Mlkl*$^{-/-}$, and *Fadd*$^{-/-}$*Mlkl*$^{-/-}$ mice 4 d after control or DOX treatment (10 mg/kg, i.p.). (*F*) Serum LDH levels were measured in control, *Mlkl*$^{-/-}$, and *Fadd*$^{-/-}$*Mlkl*$^{-/-}$ mice 4 d after control or DOX treatment (n = 6–8 mice per group). Summary data are presented as the mean ± SEM. Significance in *A*–*C* was calculated using the log-rank (Mantel–Cox) test. Significance in *D* was calculated using the Student's t test; $^{**}P < 0.01$; $^{***}P < 0.001$. Significance in *E* and *F* was calculated using a one-way ANOVA with Tukey's post hoc test; groups labeled with different letters differed significantly ($P < 0.05$). $^{*}P < 0.05$; n.s., not significant.

that Fer-1 and DXZ utilize a common mechanism in protecting against DOX-induced ferroptosis. Compared to DXZ, Fer-1 had similar effects in terms of both protecting against DOX-induced cardiac damage, as primarily evidenced by histological observation (Fig. 2 *A* and *B*). These pathological changes were accompanied by an increase in *Anp*, *Bnp*, and *Myh7* mRNA levels, three classic biomarkers of cardiac hypertrophy (Fig. 2*C*). In addition, compared with mice that were treated with DOX alone, mice that were pretreated with Fer-1 or DXZ had improved cardiac function, measured using echocardiography (Fig. 2*D* and *SI Appendix*, Fig. S2).

We also investigated the ability of Fer-1 to protect against DOX-induced cardiotoxicity in *Tg(cmlc2:GFP)* zebrafish embryos, an animal model in which the cardiomyocytes' nuclei and plasma membranes are labeled with GFP (18). We found that treating these animals with DOX decreased the heart rate and caused the heart to become distorted into an elongated shape with a compact ventricle and thin atrial wall; these effects were

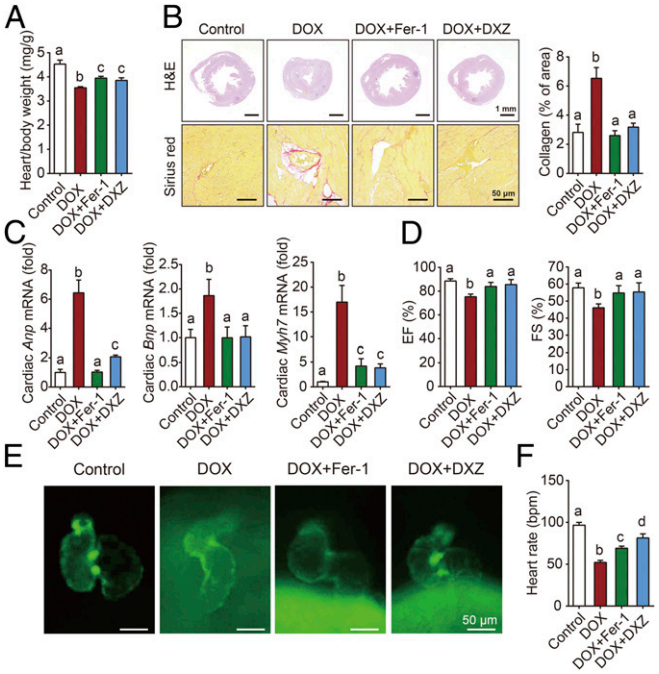

Fig. 2. Fer-1 and DXZ prevent DOX-induced cardiomyopathy. (*A*) The heart/body weight ratio was measured in control mice and mice treated with DOX with or without Fer-1 or DXZ ($n = 6$ mice per group). (*B*) Cardiac sections were prepared from control mice and mice treated with DOX with or without Fer-1 or DXZ, and then stained with hematoxylin and eosin (H&E, *Top*) or Sirius red (*Bottom*). (*C*) Relative mRNA levels of the cardiac hypertrophy biomarkers *Anp*, *Bnp*, and *Myh7* in control mice and mice treated with DOX with or without Fer-1 or DXZ ($n = 6$ mice per group). (*D*) Echocardiographic analyses of cardiac function in control mice and mice treated with DOX with or without Fer-1 or DXZ ($n = 6$ mice per group). EF, ejection fraction; FS, fractional shortening. (*E*) Representative fluorescence microscopy images of *Tg(cmlc2: GFP)* zebrafish embryos with green fluorescent protein (GFP) specifically expressed in the myocardial cells. Zebrafish [2 d postfertilization (dpf)] were exposed to 65 μM DOX in combination with Fer-1 (1 μM) and DXZ (200 μM) for 2 d. (*F*) Heart rate levels were measured in zebrafish (2 dpf) treated with DOX together with or without Fer-1 or DXZ for 2 d ($n = 6$–8 per group). Summary data are presented as the mean ± SEM. Significance was calculated using a one-way ANOVA with Tukey's post hoc test; groups labeled with different letters differed significantly ($P < 0.05$).

rescued by treating the embryos with Fer-1 and DXZ treatment (Fig. 2 *E* and *F*).

Up-Regulation of Hmox1 in DOX-Induced Ferroptosis in Murine Heart Tissues. To identify the molecular mechanism involved in DOX-induced ferroptosis, we used RNA-sequencing (RNA-seq) analysis to determine which genes are differentially expressed in the heart between DOX-treated mice and control mice (Fig. 3*A*). One day after DOX treatment, 105 genes were significantly up-regulated, while 51 genes were down-regulated. An expanded list of differentially expressed genes is provided in *SI Appendix*, Table S1. Among these genes, we found that *Hmox1* was one of the most significantly up-regulated genes (Fig. 3*B*). Real-time PCR confirmed that DOX treatment led to a significant increase in mRNA levels of *Hmox1*, but not *Hmox2*, specifically in the heart, liver, and spleen, as well as a slight but significant increase in the kidney (Fig. 3*C* and *SI Appendix*, Fig. S3), consistent with a large increase in *Ptgs2* mRNA. Consistent with increased cardiac *Hmox1* mRNA levels, we also measured increased cardiac Hmox1 protein levels in the DOX-treated mice (*SI Appendix*, Fig. S4), predominantly in the cardiomyocytes (Fig. 3*D*). Finally, we also found increased cardiac heme oxygenase activity in DOX-treated mice compared with control-treated mice (Fig. 3*E*).

To characterize the functional role of Hmox1 in the pathogenesis of DOX ferroptosis and cardiomyopathy, we treated mice with competitive Hmox1 inhibitor zinc protoporphyrin IX (ZnPP) and heme analog hemin (a Hmox1 activator). The DOX-induced increase in cardiac *Ptgs2* mRNA was blocked by ZnPP and increased by hemin (Fig. 3*F*). Similar results were observed with respect to DOX-induced changes in both serum (Fig. 3*G*) and cardiac (Fig. 3*H*) levels of malondialdehyde (MDA), the most prevalent byproduct of lipid peroxidation (19). Increased cardiac injury with oxidative stress—in the form of lipid peroxidation—was also observed by heart-to-body weight ratio, heart failure biomarkers, Sirius red staining, and immunostaining for 4-hydroxynonenal (4-HNE); and these DOX-induced changes were blocked and increased by ZnPP and hemin, respectively (Fig. 3 *I*–*K*). Thus, in vivo data in both inhibiting and activating Hmox1 indicate its essential role in DOX-induced ferroptosis and cardiomyopathy.

Nrf2/Hmox1 Pathway Mediates Heme Degradation and Releases Free Iron in Heart After DOX Administration. To explore the mechanism of Hmox1-dependent ferroptosis, we further performed KEGG enrichment analysis based on RNA-seq data. Interestingly, as one of the pathways that are affected most by DOX, the porphyrin and chlorophyll metabolic pathway was suggested to play a significant role (Fig. 4*A*). The heme oxygenase enzymes Hmox1 and Hmox2 catalyze the region-specific hydroxylation of heme to carbon monoxide, ferrous iron, and biliverdin (20). Given that *Hmox1* expression is inducible, whereas *Hmox2* is expressed constitutively (21), we hypothesized that DOX may induce localized heme degradation, in turn leading to the release of free iron.

To test this hypothesis, we first measured heme levels and found that DOX-treated mice had significantly lower levels of heme in the heart, liver, spleen, and serum compared with control-treated mice (Fig. 4 *B* and *C*). We then measured a variety of hematological parameters in control-treated and DOX-treated mice and found no difference in the number of red blood cells, but significantly lower hemoglobin levels (*SI Appendix*, Table S2) in the DOX-treated mice.

We then measured nonheme iron levels in the blood and primary organs of DOX-treated mice and found that the mice had significant accumulation of nonheme iron in the heart, liver, spleen, and blood 4 d after administration of DOX (10 mg/kg, i.p.) (Fig. 4 *D* and *E* and *SI Appendix*, Fig. S5*A*). We also found corresponding changes in the expression of iron-related genes in these organs, including *TfR1*, *FtH*, *FtL*, and *Fpn*, which encode transferrin receptor 1, ferritin H, ferritin L, and ferroportin, respectively (*SI Appendix*, Fig. S5 *B* and *C*). Hepcidin is a hepatic peptide hormone encoded by the *Hamp1* (hepcidin antimicrobial peptide 1) gene; this hormone regulates systemic iron by binding to the iron transporter ferroportin, the only known mammalian nonheme iron export protein (22). DOX-treated mice, with hepatic nonheme iron accumulation, had increased levels of hepatic *Hamp1* mRNA (*SI Appendix*, Fig. S5*D*) and a progressive loss of *Fpn* in the duodenum (*SI Appendix*, Fig. S5*E*), suggesting that the rapid increase in nonheme iron is independent of intestinal iron absorption. In addition, the increased expression of cardiac *Hamp1* mRNA (*SI Appendix*, Fig. S5*F*) also indicated local iron overload according to previous research (23). In contrast, total elemental iron levels in the heart, liver, and spleen were similar between control-treated and DOX-treated mice (Fig. 4*F*), supporting the notion that heme degradation is the principal mechanism underlying the effects of DOX treatment.

Consistently, Hmox1 inhibitor ZnPP mitigated multiorgan iron accumulation in DOX-treated mice, while loading hemin further exacerbated the situation, strongly suggesting the important

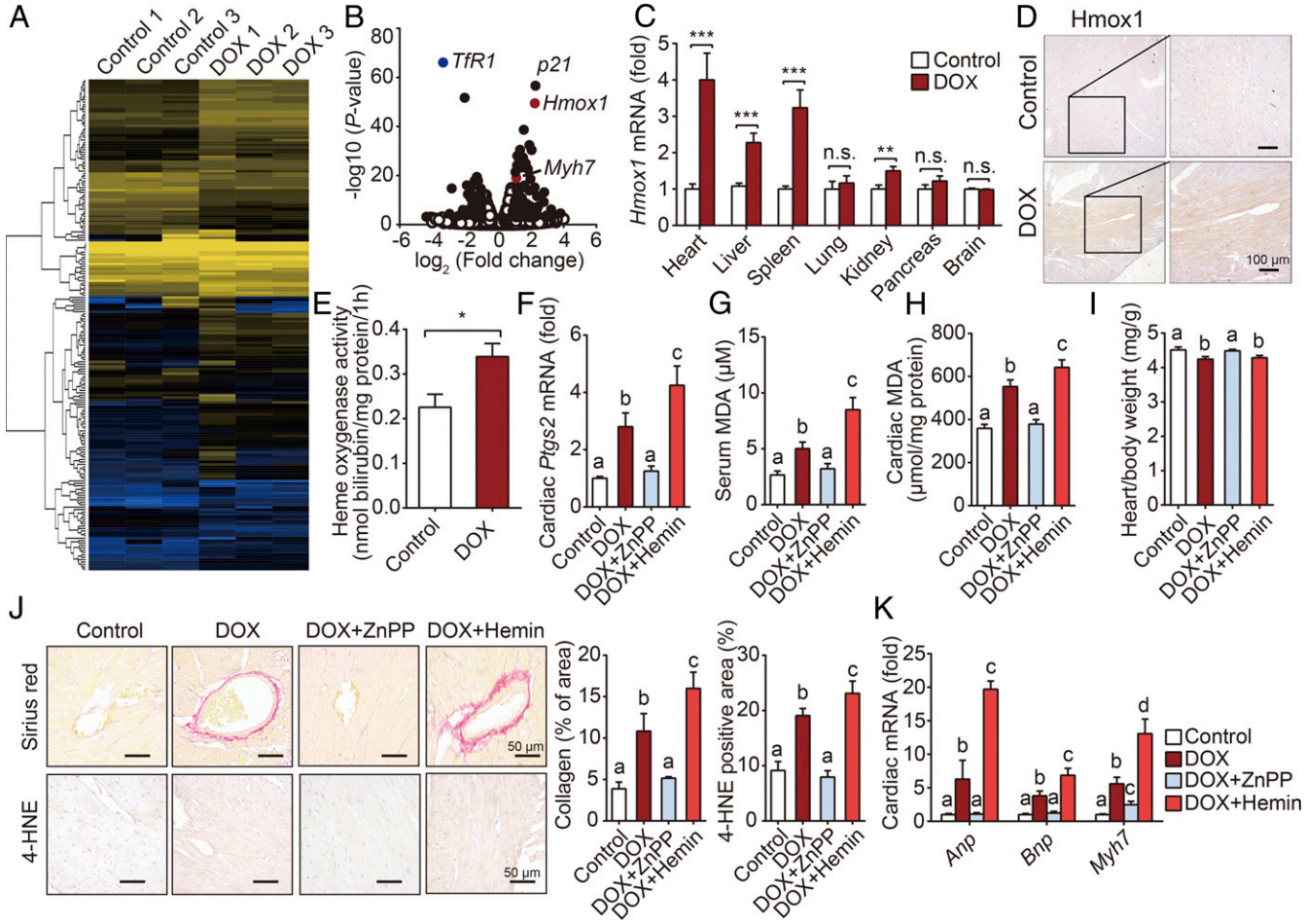

Fig. 3. Hmox1 is essential for DOX-induced ferroptosis and cardiotoxicity. (*A*) Heat map showing differentially expressed genes in cardiac tissue between control and DOX-treated mice. Low expression is depicted in blue, and high expression is depicted in yellow. (*B*) Volcano plot showing the up-regulated and down-regulated genes in response to DOX treatment measured using RNA-seq analysis. Solid symbols indicate genes in which the differential expression was statistically significant. (*C*) *Hmox1* mRNA was measured in the indicated organs of control and DOX-treated mice and is expressed relative to the respective control group ($n = 8$ mice per group). (*D*) Representative images of Hmox1-stained heart sections from control mice and DOX-treated mice. (*E*) Heme oxygenase activity was measured in heart homogenates obtained from control and DOX-treated mice ($n = 6$ mice per group). (*F–H*) Cardiac *Ptgs2* mRNA (*F*), serum MDA (*G*), and cardiac MDA (*H*) levels were measured in control mice and mice treated with DOX with or without ZnPP or hemin ($n = 6–7$ mice per group). (*I*) Heart/body weight ratio was measured in control mice and mice treated with DOX with or without ZnPP or hemin ($n = 6–7$ mice per group). (*J*) Representative images (*Left*) and quantitative analyses (*Right*) of cardiac sections stained with Sirius red (to stain collagen; *Top*) and anti–4-HNE (*Bottom*) in control mice and mice treated with DOX with or without ZnPP or hemin. (*K*) Cardiac levels of *Anp*, *Bnp*, and *Myh7* mRNA were measured in control mice and mice treated with DOX with or without ZnPP or hemin ($n = 6–7$ mice per group). Summary data are presented as the mean ± SEM. Significance in *C* and *E* was calculated using the Student's *t* test; $^*P < 0.05$; $^{**}P < 0.01$; $^{***}P < 0.001$. Significance in *F–K* was calculated using a one-way ANOVA with Tukey's post hoc test; groups labeled with different letters differed significantly ($P < 0.05$).

effect of Hmox1 in DOX-induced iron overload (*SI Appendix*, Fig. S6 *A–E*). In addition, we measured serum levels of bilirubin, a heme degradation product. Similar to the changes of iron, bilirubin accumulation in blood was observed after DOX administration, and ZnPP significantly suppressed serum bilirubin levels (*SI Appendix*, Fig. S6*F*). Interestingly, ferroptosis inhibitor Fer-1 did not reduce the DOX-induced increase in cardiac nonheme iron content; in contrast, DXZ reduced the DOX-induced increase in cardiac nonheme iron and also increased DOX-induced hepatic iron accumulation (*SI Appendix*, Fig. S7 *A–C*). Neither DXZ nor Fer-1 affected the levels of bilirubin in DOX-treated animals (*SI Appendix*, Fig. S7*D*). In other words, although Fer-1 and DXZ have similar antiferroptosis effect, they work on the heart through different mechanisms.

In vitro, treating H9c2 cells, a rat cardiomyocyte line, with DOX significantly up-regulated *Ptgs2* mRNA levels (*SI Appendix*, Fig. S8*A*). Among a panel of anthracyclines, DOX had the strongest effect on *Ptgs2* expression in cardiomyocytes, causing a fivefold increase in *Ptgs2* mRNA compared with control-treated cells (*SI Appendix*, Fig. S8*B*). Importantly, this increase in *Ptgs2* expression was prevented by treating cells with either Fer-1 or DXZ, whereas the apoptosis inhibitor zVAD had no effect (*SI Appendix*, Fig. S8*C*). DOX-induced cell death was increased by cotreating cells with ferric citrate (FAC), and this effect was reduced by Fer-1, but not zVAD (*SI Appendix*, Fig. S8*D*). However, consistent with previous results (3, 24), we found that DOX-induced cell death could not be rescued in vitro using either iron/metal chelators or Fer-1 (*SI Appendix*, Fig. S8*D*). This apparent discrepancy between our in vivo and in vitro results might be due to absence of the heme–Hmox1 iron cascade in cultured cardiomyocytes—and thus limited lipid peroxidation under in vitro conditions (*SI Appendix*, Fig. S8*E*). Consistent with the apoptosis inhibitor zVAD having no effect on DOX-induced cell death, we found that although DOX treatment increased caspase-3/7 activity in H9c2 cells, FAC cotreatment had no

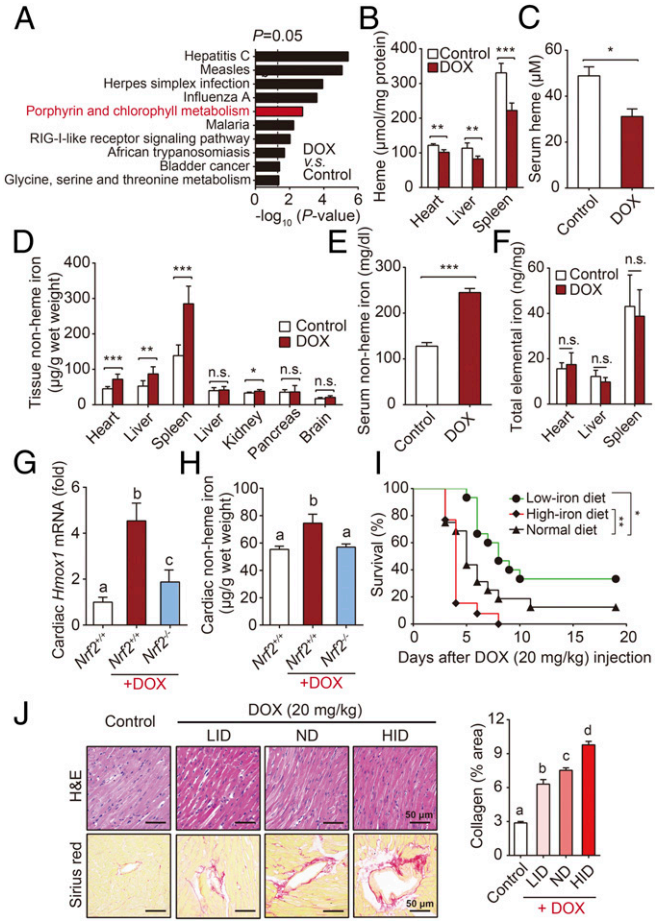

Fig. 4. Free iron released from heme degradation by Nrf2/Hmox1 pathway triggers cardiac injury. (*A*) KEGG pathway analysis of RNA-seq data. (*B* and *C*) Heme levels in the heart, liver, and spleen (*B*), and serum heme levels (*C*) were measured in mice injected with DOX (10 mg/kg, i.p.) or saline (control) for 4 d ($n = 8$ mice per group). (*D* and *E*) Nonheme iron levels in the heart, liver, spleen, lung, kidney, pancreas, and brain (*D*), and serum nonheme iron levels (*E*) were measured in mice injected with DOX (10 mg/kg, i.p.) or saline (control) for 4 d ($n = 8$ mice per group). (*F*) Total tissue iron levels were measured 4 d after DOX or control treatment ($n = 8$ mice per group). (*G* and *H*) Relative *Hmox1* mRNA (*G*) and nonheme iron (*H*) levels in the hearts were measured in WT mice, DOX-treated $Nrf2^{-/-}$ and $Nrf2^{+/+}$ mice, $n = 4$–6 mice per group. (*I*) Kaplan–Meier survival curves of mice fed a low-iron diet, normal diet, or high-iron diet, then injected with DOX (20 mg/kg, i.p.) ($n = 13$–16 mice per group). (*J*) Cardiac tissue sections were prepared from the mice in *D* and stained with H&E (*Top*) or Sirius red (*Bottom*). Control mice were fed a normal diet and were not treated with DOX. Summary data are presented as the mean ± SEM. Significance in *B*–*F* was calculated using the Student's *t* test; $^*P < 0.05$; $^{**}P < 0.01$; $^{***}P < 0.001$. Significance in *G*, *H*, and *J* was calculated using a one-way ANOVA with Tukey's post hoc test; groups labeled with different letters differed significantly ($P < 0.05$). Significance in *I* was calculated using the log-rank (Mantel–Cox) test.

further effect, and zVAD treatment reduced caspase-3/7 activity to control levels (*SI Appendix*, Fig. S8*F*).

Hmox1 expression is induced by activation of the redox-sensitive transcription factor Nrf2 (nuclear factor erythroid 2-related factor 2) (25). Upon translocating to the nucleus, Nrf2 binds to the antioxidant response element (ARE) in the upstream promoter region of several antioxidative genes—including *Hmox1*—thereby initiating their transcription (26). Consistent with previous reports (27), DOX treatment led to an increase in nuclear Nrf2 protein levels (*SI Appendix*, Fig. S9*A*) and increased myocardial *Nrf2* mRNA levels (*SI Appendix*, Fig. S9*B*). Furthermore, DOX-treated *Nrf2* knockout mice ($Nrf2^{-/-}$, see *SI Appendix*, Fig. S9*C*) have reduced cardiac *Hmox1* mRNA levels compared with DOX-treated wild-type mice (Fig. 4*G*), consistent with Nrf2 activation playing an essential role in mediating the effects of DOX on *Hmox1* expression. In addition, cardiac nonheme iron differed significantly between DOX-treated wild-type mice and DOX-treated $Nrf2^{-/-}$ mice (Fig. 4*H*). Thus, DOX augments the nuclear accumulation of Nrf2 and enables Nrf2 to promote Hmox1 expression, which leads to degradation of heme and release of free iron in heart.

We next determined whether iron overload is essential to trigger cardiac ferroptosis. We fed male C57BL/6 mice a diet containing various nutritional iron levels and then injected these mice with DOX. Consistent with previous reports (28), mice that were fed a high-iron diet (HID) developed more severe DOX-induced cardiotoxicity, reflected by increased mortality and more severe heart damage compared with mice that were fed a normal-iron diet; in contrast, mice that were fed a low-iron diet (LID) had significantly lower DOX-induced mortality and less severe heart damage (Fig. 4 *I* and *J*).

Fer-1 and DXZ Protect Against DOX-Induced Cardiomyopathy by Maintaining Mitochondrial Function. Emerging evidence suggests that ferroptosis represents a vulnerability caused by the incorporation of polyunsaturated fatty acids into cellular membranes (4). However, there are still several key questions in the lipid peroxidation process that drives ferroptosis, one of which is the location in which lipid peroxidation takes place during ferroptosis (29). Does this event occur in the plasma membrane, nuclear membrane, mitochondria, endoplasmic reticulum, lysosome, or other lipid membranes in the cell? To address this question, we observed hearts of DOX-treated mice using transmission electron microscopy.

As a result, our analysis revealed that the myocardial mitochondria in DOX-treated mice were severely distorted and enlarged, and these DOX-induced effects were rescued by both Fer-1 and DXZ treatment (Fig. 5*A*). Mitochondria serve as the powerhouse of cardiomyocytes, where their primary function is to synthesize ATP via oxidative phosphorylation. However, this process of generating ATP through the respiratory chain results in the production of reactive oxygen species as a metabolic byproduct (30). Fer-1 also reversed the DOX-induced decrease in the expression of the mitochondrial genes *mt-Cytb* and *mt-Atp6* (Fig. 5*B*), as well as the DOX-induced decrease in ATP production (Fig. 5*C*), suggesting that inhibiting ferroptosis can protect mitochondrial function. In addition, Western blot analyses of the proteins in the respiratory chain complex in cardiac tissue revealed that both complex I and complex II were decreased following DOX treatment, and these changes were reversed by both Fer-1 and DXZ treatment (*SI Appendix*, Fig. S10*A*).

Mitochondrial membrane potential ($\Delta\Psi m$) is commonly used to measure mitochondrial function, with a loss of $\Delta\Psi m$ indicating mitochondrial dysfunction (31). The presence of an electrochemical potential gradient in healthy mitochondria drives accumulation of the dye JC-1 in the mitochondrial matrix, forming red fluorescent aggregates in healthy cells; a loss of $\Delta\Psi m$ prevents this accumulation in the mitochondria, leading to a shift in fluorescence from red (JC-1 aggregates) to green (JC-1 monomers). Based on this analysis, we found that cardiomyocytes in DOX-treated mice have significantly more JC-1 monomers compared with control-treated mice, consistent with reduced mitochondrial $\Delta\Psi m$ (Fig. 5*D*); moreover, both Fer-1 and DXZ reduced this DOX-induced effect, presumably by maintaining mitochondrial $\Delta\Psi m$. To further examine the role that mitochondria play in DOX-induced ferroptosis, we isolated subcellular fractions of cardiomyocytes and found that DOX treatment significantly increased lipid peroxidation (Fig. 5*E*) and nonheme iron (Fig. 5*F*) specifically in the mitochondria, but not in the cytoplasm.

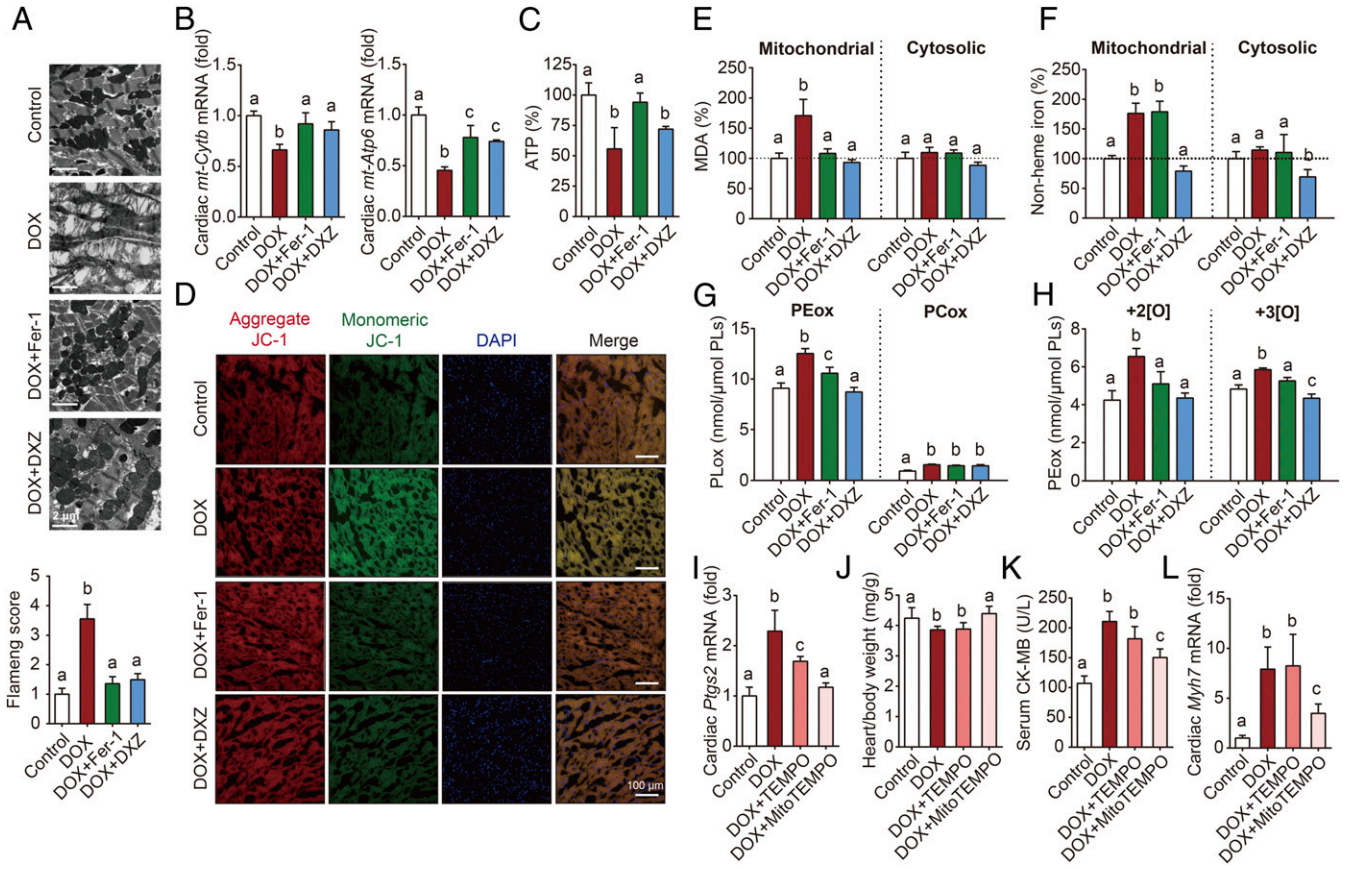

Fig. 5. Mitochondrial iron overload and lipid peroxidation play a key role in DOX-induced myocardial ferroptosis. (*A*) Representative transmission electron microscopy images and corresponding relative Flameng scores (*Bottom*) for cardiac tissue obtained from control and mice treated with DOX with or without Fer-1 or DXZ. (*B* and *C*) Cardiac *mt-Cytb* and *mt-Atp6* mRNA levels (*B*) and cardiac ATP (*C*) were measured in control mice and mice treated with DOX with or without Fer-1 or DXZ (n = 6–7 mice per group). (*D*) Representative images of cardiac JC-1 fluorescence in control mice and mice treated with DOX with or without Fer-1 or DXZ. (*E* and *F*) Cardiac mitochondrial and cytosolic MDA levels (*E*) and mitochondrial and cytosolic nonheme iron (*F*) were measured in control mice and mice treated with DOX with or without Fer-1 or DXZ (n = 6–7 mice per group). (*G* and *H*) Cardiac PEox and PCox (*G*) and dioxide and trioxide PEox species (*H*) were measured in control mice and DOX mice treated with or without Fer-1 or DXZ. (*I*–*L*) Cardiac *Ptgs2* mRNA (*I*), the heart/body weight ratio (*J*), serum CK-MB levels (*K*), and cardiac *Myh7* mRNA (*L*) were measured in control mice and mice treated with DOX with or without TEMPO or MitoTEMPO (n = 6 mice per group). Summary data are presented as the mean ± SEM. Significance was calculated using a one-way ANOVA with Tukey's post hoc test; groups labeled with different letters differed significantly ($P < 0.05$).

Previous studies showed that phosphatidylethanolamines (PEs) are key phospholipids (PLs) that undergo oxidation, driving ferroptosis (32, 33). To investigate whether DOX induces the oxidation of mitochondrial PEs, we performed global redox phospholipidomics LC-MS/MS analyses in isolated cardiac mitochondria. Our analysis revealed that oxygenated PE (PEox), including both dioxide and trioxide PEox species, were more abundant in cardiac mitochondria than oxygenated phosphatidylcholine (PCox), and DOX treatment significantly increased the levels of PEox (Fig. 5 *G* and *H*). Moreover, treating the mice with either Fer-1 or DXZ significantly blocked the DOX-induced increase in PEox (Fig. 5 *G* and *H*).

Next, we tested whether mitochondrial lipid peroxidation plays a pathogenic role in DOX-induced ferroptosis and cardiotoxicity by measuring the effects of MitoTEMPO, a mitochondria-targeted antioxidant. We found that MitoTEMPO abolished DOX-induced lipid peroxidation (*SI Appendix*, Fig. S10*B*) and cardiac ferroptosis (Fig. 5*I*); in contrast, the nonmitochondria-targeted version (TEMPO) only mildly rescued the DOX-induced effects. Moreover, MitoTEMPO, but not TEMPO, significantly reduced DOX-induced cardiomyopathy assessed by measuring the heart/body weight ratio, serum levels of myocardial enzymes, and cardiac hypertrophy biomarkers (Fig. 5 *J*–*L* and *SI Appendix*, Fig. S10 *C*–*E*). In contrast, neither Mito-TEMPO nor TEMPO affected the DOX-induced increase in cardiac and systemic nonheme iron levels (*SI Appendix*, Fig. S10 *F* and *G*).

Blocking Ferroptosis Reduces the Severity of Cardiac Ischemia/Reperfusion Injury. Cardiac I/R injury is also associated with a loss of cardiomyocytes and subsequent heart failure. Compared with sham-operated mice, mice that were subjected to 30 min of myocardial ischemia followed by 24 h of reperfusion had significantly higher levels of cardiac nonheme iron (Fig. 6*A*) and *Ptgs2* mRNA (Fig. 6*B*). In addition, both cardiac *FtH* and cardiac *FtL* mRNA levels were higher in the I/R group compared with the sham group (*SI Appendix*, Fig. S11 *A* and *B*); in contrast, I/R had no effect on either serum nonheme iron or transferrin saturation (*SI Appendix*, Fig. S11 *C* and *D*). Given the clinical similarities between DOX treatment and I/R, we tested whether inhibiting ferroptosis can also protect against the effects of I/R.

Mice were pretreated with either the ferroptosis inhibitor Fer-1 or the iron chelator DXZ, and then subjected to I/R (*SI Appendix*, Fig. S11*E*). Our analysis revealed that both Fer-1 and DXZ pretreatment significantly reduced myocardial infarct size, although the groups had comparable areas at risk (Fig. 6*C*). In addition, both Fer-1 and DXZ pretreatment prevented the

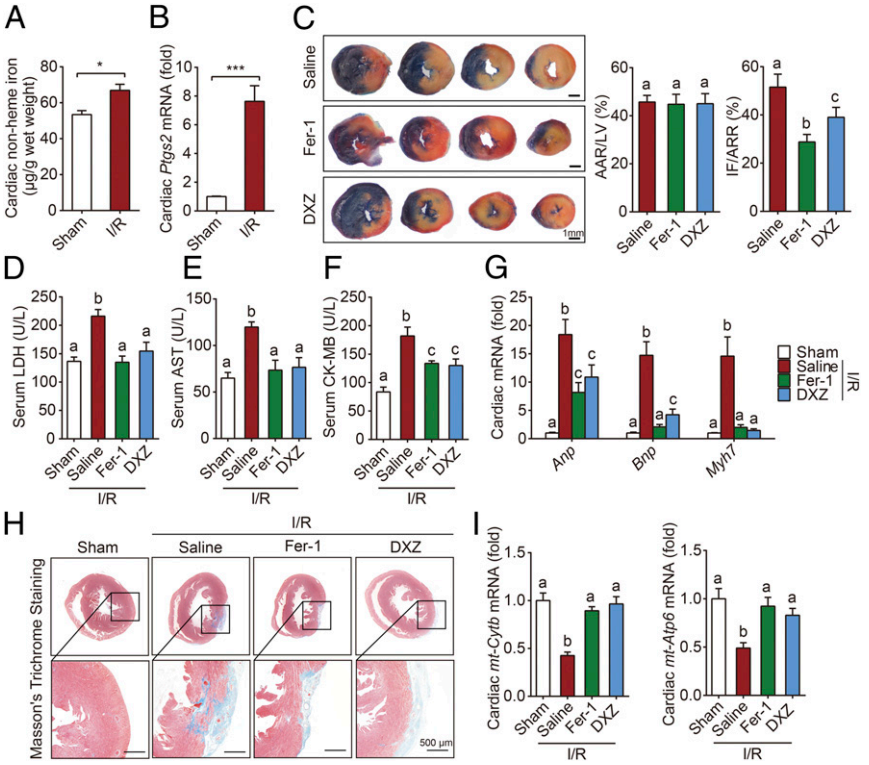

Fig. 6. Blocking ferroptosis protects the heart against I/R injury. (*A* and *B*) Cardiac nonheme iron levels (*A*) and cardiac *Ptgs2* mRNA levels (*B*) were measured in mice subjected to sham surgery or 30-min cardiac ischemia followed by 24 h of reperfusion (I/R) (n = 6–8 mice per group). (*C*) Representative images (*Left*) and quantitative data (*Right*) for infarct size (IF) and relative area at risk (AAR) in heart sections obtained from mice subjected to 30 min/24 h I/R injury and treated with saline (control), Fer-1, or DXZ. (*D*–*G*) Serum LDH levels (*D*), AST levels (*E*), CK-MB levels (*F*), and cardiac *Anp*, *Bnp*, and *Myh7* mRNA (*G*) measured in mice subjected to sham surgery or 30 min/24 h I/R injury and treated with saline, Fer-1, or DXZ (n = 6–8 mice per group). (*H*) Representative images of Masson's trichrome staining of heart sections obtained from mice subjected to sham surgery or 30 min/4 wk I/R injury and treated with saline, Fer-1, or DXZ. (*I*) Cardiac *mt-Cytb* and *mt-Atp6* mRNA levels were measured in mice subjected to sham surgery or 30 min/24 h I/R injury and treated with saline, Fer-1, or DXZ (n = 6–8 mice per group). Summary data are presented as the mean ± SEM. Significance in *A* and *B* was calculated using the Student's t test; $^{*}P < 0.05$; $^{***}P < 0.001$. Significance in *C*–*G* and *I* was calculated using a one-way ANOVA with Tukey's post hoc test; groups labeled with different letters differed significantly ($P < 0.05$).

I/R-induced increase in myocardial enzymes measured in the serum, including lactate dehydrogenase (LDH), aspartate transaminase (AST), and creatine kinase-MB isoenzyme (CK-MB) (Fig. 6 *D*–*F*). Moreover, both Fer-1 and DXZ pretreatment prevented the I/R-induced increase in *Anp*, *Bnp*, and *Myh7* mRNA levels (Fig. 6*G*). Taken together, these results suggest that blocking ferroptosis can protect the heart from the effects of ischemia/reperfusion.

Finally, we examined whether blocking ferroptosis and iron chelation therapy can provide long-term protection from I/R injury. Mice were pretreated with Fer-1 or DXZ, and then subjected to 30 min of myocardial ischemia followed by 4 wk of reperfusion, during which the mice received an injection of Fer-1 or DXZ every 2 d (*SI Appendix*, Fig. S11*F*). We found that both I/R-induced cardiac remodeling and fibrosis (Fig. 6*H* and *SI Appendix*, Fig. S11*G*) were significantly reduced in the treated groups. Moreover, the I/R-induced decrease in cardiac *mt-Cytb* and *mt-Atp6* mRNA levels was prevented in both the Fer-1 and DXZ groups (Fig. 6*I*), suggesting that inhibiting ferroptosis can provide significant protection against the effects of myocardial I/R, presumably by maintaining mitochondrial function.

Discussion

Cardiovascular disease remains one of the leading causes of death worldwide. Here, we systematically studied the role of ferroptosis, a recently discovered iron-dependent form of cell death, in cardiac injury induced by either the anticancer drug doxorubicin or cardiac ischemia/reperfusion. We found that the inducible heme oxygenase Hmox1 is up-regulated by the nuclear translocation of Nrf2 in DOX-induced cardiac injury, catalyzing heme degradation and facilitating the release of free iron, leading to ferroptosis and ultimately heart failure. Notably, inhibiting either ferroptosis or Hmox1 significantly reduced DOX-induced cardiac injury and heart failure, similar to the protective effects of iron chelation with DXZ. Moreover, inhibiting ferroptosis significantly reduced I/R-related cardiac injury, suggesting a potential therapeutic approach for treating and/or preventing ischemic heart damage.

Preventing cardiac cell death has been suggested to be an effective cardioprotective strategy (34). During cardiac injury, caspase-dependent apoptosis has long been accepted as the major form of regulated cell death in cardiomyocytes. Interestingly, however, several other regulatory mechanisms and signaling pathways that govern necrotic cell death have also been implicated in cardiac injury (2). For example, Zhang et al. (13) recently reported that Ripk3-dependent necroptosis plays a role in both ischemia/reperfusion and DOX-induced cardiac injury, indicating that several forms of cardiac cell death—and their underlying mechanisms—likely play a role in this process. Notably, unlike the previous report, we found that pharmacologic inhibition of CaMKII, a key RIPK3 substrate mediating myocardial necroptosis, had no effect on DOX-induced mortality in our study. It is postulated that genetic CaMKII deletion holds the promise for better understanding the role of CaMKII in cardiomyopathy.

Here, we report that ferroptosis plays an important role in DOX-induced cardiotoxicity. Ferroptosis is a recently identified iron-dependent, nonapoptotic form of cell death that can be prevented or even reversed using iron chelation (3, 35, 36). Importantly, ferroptosis is morphologically, biochemically, and genetically distinct from both apoptosis and necroptosis. We found that DOX triggers the accumulation of mitochondrial iron in cardiomyocytes, which in turn damages lipid membranes, particularly the mitochondrial membranes.

In both animal models and patients, iron overload plays a pathogenic role in cardiotoxicity in several cardiopathic conditions (37). In this study, we found that feeding mice a low-iron diet reduced DOX-induced cardiotoxicity and increased survival, suggesting that targeting cardiac iron metabolic pathways may be clinically relevant. In addition, we found that the accumulation of iron in both serum and cardiac tissue is driven by the rapid conversion of heme to free iron via up-regulation of Hmox1 in a process independent of the canonical hepcidin–ferroportin iron regulatory axis.

Paradoxically, Hmox1 is widely considered to be a robust cardioprotective protein, as overexpressing Hmox1 in mice can protect against both cardiac ischemia/reperfusion injury and permanent coronary ligation-induced heart failure (38, 39). On the other hand, transgenic mice that overexpress Hmox1—but not wild-type littermates—develop spontaneous heart failure at 1 y of age (40). Moreover, altered Hmox1 activity has been reported to play a protective role in both hyperoxia-induced and bleomycin-induced lung injury (41, 42) and in brain injury following intracerebral hemorrhage (43). These findings underscore the pathogenic role that Hmox1 plays in a variety of tissues and processes.

Our results support the notion that DOX-induced iron accumulation and DOX-induced cardiomyopathy are mediated by Hmox1. Hmox1 expression is regulated by several transcription factors, including *Nrf2*, *AP-1*, *YY1*, and *Hif1α* (21), and we found that *Nrf2*-deficient mice are resistant to DOX-induced Hmox1 up-regulation and iron accumulation. However, these mice develop cardiac dysfunction (27), suggesting that the local effect of deleting *Nrf2* in the heart may differ from the global effect of deleting *Nrf2*.

Interestingly, although the potent iron chelator deferoxamine is used to treat iron overload diseases such as thalassemia and sickle cell disease, its protective effect with respect to cardiac injury is unclear (44). One possible explanation for this discrepancy is that DXZ—but not deferoxamine—may decrease mitochondrial iron content in response to DOX, thereby protecting against DOX-induced cardiotoxicity (15).

MitoTEMPO, a superoxide scavenger designed to target the mitochondria, can readily pass through lipid bilayers and accumulates selectively in mitochondria (45). Here, we found that MitoTEMPO—but not TEMPO, which does not specifically target any subcellular structures—potently suppressed DOX-induced ferroptosis in cardiac cells by scavenging lipid peroxidation specifically in the mitochondria, providing cardioprotective benefits similar to the effects of Fer-1. This finding supports the notion that mitochondrial lipid peroxidation due to mitochondrial iron accumulation plays a key role in cardiac ferroptosis.

Notably, we found that cardiac ischemia/reperfusion in mice leads to mitochondrial iron accumulation. Importantly, both blocking ferroptosis and chelating iron were cardioprotective in a mouse model of myocardial I/R injury. This is consistent with a previous report that MitoQ, a mitochondria-targeted antioxidant, significantly reduced cardiac I/R-related heart dysfunction, cell death, and mitochondrial damage, whereas an untargeted antioxidant did not confer cardioprotection (46).

It is currently under debate whether mitochondria are involved in ferroptosis. Aberrant morphological changes of mitochondria have been initially observed in HT-1080 cells treated with erastin, a ferroptosis activator (3). By contrast, it is reported that mitochondria-deficient cells were still sensitive to ferroptosis (47). Most recently, Gao et al. (48) reported that mitochondria are important for cysteine deprivation-induced ferroptosis but not in glutathione peroxidase-4 (GPX4) inhibition-induced ferroptosis. In this study, we demonstrated that mitochondria play an essential role in doxorubicin- and ischemia/reperfusion-induced ferroptosis in cardiomyocytes in vivo, which provides insights into better understanding the underlying molecular mechanism of ferroptosis in triggering pathogenesis of cardiomyopathy.

In summary, we report a mechanism by which ferroptosis mediates the pathogenesis of DOX-induced cardiotoxicity and I/R-mediated cardiomyopathy via the Nrf2/Hmox1 axis. Our findings suggest that selectively inhibiting ferroptosis in cardiomyocytes may represent a feasible therapeutic approach for managing DOX-induced cardiac injury without compromising the drug's anticancer properties. Moreover, our in vivo data support the notion that decreasing mitochondrial iron accumulation and/or inhibiting lipid peroxidation is cardioprotective during both acute and chronic cardiac I/R. From a clinical perspective, these findings indicate that treating cardiomyopathy by inhibiting ferroptosis may help prevent iron overload-induced heart failure. Future studies are needed to test the potential clinical implications of this therapeutic strategy.

Materials and Methods

All animal procedures were approved by the Animal Care and Use Committee of Zhejiang University. The generation of *Ripk3*$^{-/-}$, *Mlkl*$^{-/-}$, *Fadd*$^{-/-}$*Mlkl*$^{-/-}$, and *Nrf2*$^{-/-}$ mice (17, 49, 50), LC/MS analysis, iron assay, and methods used in surgery, drug treatment, cell culture, histology, lipid peroxidation detection, and mitochondria isolation are provided in *SI Appendix, SI Materials and Methods*. Except where indicated otherwise, all summary data are presented as the mean ± SEM. The Student's *t* test was used to compare two groups, and the log-rank test was used to analyze the survival curves. Differences with a *P* value of <0.05 were considered statistically significant.

ACKNOWLEDGMENTS. We thank Drs. Xiaodong Wang, Yan Zhang, and Rui-Ping Xiao for providing the *Ripk3*$^{-/-}$ mice; Dr. Haibing Zhang for providing the *Fadd*$^{-/-}$*Mlkl*$^{-/-}$ mice; Drs. Masayuki Yamamoto and Jingbo Pi for providing *Nrf2*$^{-/-}$ mice; Dr. Bo Zhang for providing the *Tg(cmlc2:gfp)* zebrafish; and Shenyan Liu, Wei Bi, Jifeng Wang, Peng An, and Qian Wu for their suggestions or execution of some in vivo studies. This study was supported by research grants from the National Key Research and Development Program (2018YFA0507802 to F.W. and 2018YFA0507801 to J.M.) and the National Natural Science Foundation of China (31330036 and 31530034 to F.W., 31570791 and 91542205 to J.M., and 31701035 to H.W.).

1. Fuchs Y, Steller H (2011) Programmed cell death in animal development and disease. *Cell* 147:742–758.
2. Conrad M, Angeli JP, Vandenabeele P, Stockwell BR (2016) Regulated necrosis: Disease relevance and therapeutic opportunities. *Nat Rev Drug Discov* 15: 348–366.
3. Dixon SJ, et al. (2012) Ferroptosis: An iron-dependent form of nonapoptotic cell death. *Cell* 149:1060–1072.
4. Stockwell BR, et al. (2017) Ferroptosis: A regulated cell death nexus linking metabolism, redox biology, and disease. *Cell* 171:273–285.
5. Linkermann A, et al. (2014) Synchronized renal tubular cell death involves ferroptosis. *Proc Natl Acad Sci USA* 111:16836–16841.
6. Tuo QZ, et al. (2017) Tau-mediated iron export prevents ferroptotic damage after ischemic stroke. *Mol Psychiatry* 22:1520–1530.
7. Young RC, Ozols RF, Myers CE (1981) The anthracycline antineoplastic drugs. *N Engl J Med* 305:139–153.
8. Singal PK, Iliskovic N (1998) Doxorubicin-induced cardiomyopathy. *N Engl J Med* 339: 900–905.
9. Swain SM, Whaley FS, Ewer MS (2003) Congestive heart failure in patients treated with doxorubicin: A retrospective analysis of three trials. *Cancer* 97:2869–2879.
10. Nabhan C, et al. (2015) Disease characteristics, treatment patterns, prognosis, outcomes and lymphoma-related mortality in elderly follicular lymphoma in the United States. *Br J Haematol* 170:85–95.
11. Arola OJ, et al. (2000) Acute doxorubicin cardiotoxicity involves cardiomyocyte apoptosis. *Cancer Res* 60:1789–1792.
12. Lu L, et al. (2009) Adriamycin-induced autophagic cardiomyocyte death plays a pathogenic role in a rat model of heart failure. *Int J Cardiol* 134:82–90.
13. Zhang T, et al. (2016) CaMKII is a RIP3 substrate mediating ischemia- and oxidative stress-induced myocardial necroptosis. *Nat Med* 22:175–182.
14. Wang Y, et al. (2017) Chemotherapy drugs induce pyroptosis through caspase-3 cleavage of a gasdermin. *Nature* 547:99–103.

15. Ichikawa Y, et al. (2014) Cardiotoxicity of doxorubicin is mediated through mitochondrial iron accumulation. *J Clin Invest* 124:617–630.
16. Yang WS, et al. (2014) Regulation of ferroptotic cancer cell death by GPX4. *Cell* 156: 317–331.
17. Zhang X, et al. (2016) MLKL and FADD are critical for suppressing progressive lymphoproliferative disease and activating the NLRP3 inflammasome. *Cell Rep* 16: 3247–3259.
18. Huang CJ, Tu CT, Hsiao CD, Hsieh FJ, Tsai HJ (2003) Germ-line transmission of a myocardium-specific GFP transgene reveals critical regulatory elements in the cardiac myosin light chain 2 promoter of zebrafish. *Dev Dyn* 228:30–40.
19. Wang H, et al. (2017) Characterization of ferroptosis in murine models of hemochromatosis. *Hepatology* 66:449–465.
20. Maines MD (1997) The heme oxygenase system: A regulator of second messenger gases. *Annu Rev Pharmacol Toxicol* 37:517–554.
21. Ayer A, Zarjou A, Agarwal A, Stocker R (2016) Heme oxygenases in cardiovascular health and disease. *Physiol Rev* 96:1449–1508.
22. Ganz T (2013) Systemic iron homeostasis. *Physiol Rev* 93:1721–1741.
23. Lakhal-Littleton S, et al. (2016) An essential cell-autonomous role for hepcidin in cardiac iron homeostasis. *eLife* 5:e19804.
24. Shimada K, et al. (2016) Global survey of cell death mechanisms reveals metabolic regulation of ferroptosis. *Nat Chem Biol* 12:497–503.
25. Alam J, et al. (1999) Nrf2, a Cap'n'Collar transcription factor, regulates induction of the heme oxygenase-1 gene. *J Biol Chem* 274:26071–26078.
26. McMahon M, Itoh K, Yamamoto M, Hayes JD (2003) Keap1-dependent proteasomal degradation of transcription factor Nrf2 contributes to the negative regulation of antioxidant response element-driven gene expression. *J Biol Chem* 278:21592–21600.
27. Li S, et al. (2014) Nrf2 deficiency exaggerates doxorubicin-induced cardiotoxicity and cardiac dysfunction. *Oxid Med Cell Longev* 2014:748524.
28. Panjrath GS, et al. (2007) Potentiation of doxorubicin cardiotoxicity by iron loading in a rodent model. *J Am Coll Cardiol* 49:2457–2464.
29. Feng H, Stockwell BR (2018) Unsolved mysteries: How does lipid peroxidation cause ferroptosis? *PLoS Biol* 16:e2006203.
30. Chen YR, Zweier JL (2014) Cardiac mitochondria and reactive oxygen species generation. *Circ Res* 114:524–537.
31. Skárka L, Ostádal B (2002) Mitochondrial membrane potential in cardiac myocytes. *Physiol Res* 51:425–434.
32. Kagan VE, et al. (2017) Oxidized arachidonic and adrenic PEs navigate cells to ferroptosis. *Nat Chem Biol* 13:81–90.
33. Doll S, et al. (2017) ACSL4 dictates ferroptosis sensitivity by shaping cellular lipid composition. *Nat Chem Biol* 13:91–98.
34. Whelan RS, Kaplinskiy V, Kitsis RN (2010) Cell death in the pathogenesis of heart disease: Mechanisms and significance. *Annu Rev Physiol* 72:19–44.
35. Angeli JPF, Shah R, Pratt DA, Conrad M (2017) Ferroptosis inhibition: Mechanisms and opportunities. *Trends Pharmacol Sci* 38:489–498.
36. Jiang L, et al. (2015) Ferroptosis as a p53-mediated activity during tumour suppression. *Nature* 520:57–62.
37. Gujja P, Rosing DR, Tripodi DJ, Shizukuda Y (2010) Iron overload cardiomyopathy: Better understanding of an increasing disorder. *J Am Coll Cardiol* 56:1001–1012.
38. Yet SF, et al. (2001) Cardiac-specific expression of heme oxygenase-1 protects against ischemia and reperfusion injury in transgenic mice. *Circ Res* 89:168–173.
39. Wang G, et al. (2010) Cardioprotective and antiapoptotic effects of heme oxygenase-1 in the failing heart. *Circulation* 121:1912–1925.
40. Allwood MA, et al. (2014) Heme oxygenase-1 overexpression exacerbates heart failure with aging and pressure overload but is protective against isoproterenol-induced cardiomyopathy in mice. *Cardiovasc Pathol* 23:231–237.
41. Dennery PA, et al. (2003) Resistance to hyperoxia with heme oxygenase-1 disruption: Role of iron. *Free Radic Biol Med* 34:124–133.
42. Atzori L, et al. (2004) Attenuation of bleomycin induced pulmonary fibrosis in mice using the heme oxygenase inhibitor Zn-deuteroporphyrin IX-2,4-bisethylene glycol. *Thorax* 59:217–223.
43. Wang J, Doré S (2007) Heme oxygenase-1 exacerbates early brain injury after intracerebral haemorrhage. *Brain* 130:1643–1652.
44. Elihu N, Anandasbapathy S, Frishman WH (1998) Chelation therapy in cardiovascular disease: Ethylenediaminetetraacetic acid, deferoxamine, and dexrazoxane. *J Clin Pharmacol* 38:101–105.
45. Dikalova AE, et al. (2010) Therapeutic targeting of mitochondrial superoxide in hypertension. *Circ Res* 107:106–116.
46. Adlam VJ, et al. (2005) Targeting an antioxidant to mitochondria decreases cardiac ischemia-reperfusion injury. *FASEB J* 19:1088–1095.
47. Gaschler MM, et al. (2018) Determination of the subcellular localization and mechanism of action of ferrostatins in suppressing ferroptosis. *ACS Chem Biol* 13: 1013–1020.
48. Gao M, et al. (December 13, 2018) Role of mitochondria in ferroptosis. *Mol Cell*, 10.1016/j.molcel.2018.10.042.
49. He S, et al. (2009) Receptor interacting protein kinase-3 determines cellular necrotic response to TNF-alpha. *Cell* 137:1100–1111.
50. Itoh K, et al. (1997) An Nrf2/small Maf heterodimer mediates the induction of phase II detoxifying enzyme genes through antioxidant response elements. *Biochem Biophys Res Commun* 236:313–322.